Thermodynamic Advantage of Transient Wave Dynamics in Hierarchical Decision Architectures.

Coherent Resonant Netting (CRN) via an Open-System Formalism

Oleg Dolgikh

Independent Researcher, Sant Cugat del Vallès, Spain

ORCID: 0009-0008-0159-1718

Correspondence: hanlon@occam.world

Article type: Hypothesis & Theory

Word count (main text, excl. references): 8594. Figures: 8. Tables: 1. Supplementary Notes: 6. Supplementary Figures: 3.

Abstract

We propose Coherent Resonant Netting (CRN), a two-stage decision architecture designed for communication-dominant neural energetics. A transient wave-like pre-selection episode runs on an active hypothesis graph, pruning inconsistent candidates by phase-sensitive interference, before a thresholded fixation/broadcast stage commits to a discrete winner. The core engineering motivation is the strong asymmetry $E_{comm} \gg E_{comp}$: long-range spiking and broadcast are metabolically expensive relative to local subthreshold dynamics, so the relevant objective is information-per-spike rather than raw wall-clock speed in the reset-limited regime. Stage I is formalized as open-system wave transport on graphs using a GKSL/Lindblad generator (used here as a mesoscopic tool, not as a claim of microscopic quantum coherence). This yields operational markers: a Liouvillian spectral-gap maximum $g(\kappa)$, a broad intermediate-noise noise-assisted transport (NAT/ENAQT-like) window W_κ, and an energy-checkpoint ratio χ that bounds when wave-layer maintenance remains well below the cost of additional spike/broadcast events. Reproducible simulations across toy and large graphs, and matched classical random-walk baselines, show interference trapping at low noise and its noise-assisted release within the NAT window. Finally, we outline falsifiable signatures (P1-P6) and dissociation protocols (Drosophila and mammalian/EEG/MEG extensions) to test CRN's architectural predictions.

Keywords: active inference; neuroenergetics; information thermodynamics; open-system dynamics; Lindblad master equation; noise-assisted transport; spectral gap; decision architectures

Contribution to the Field

Coherent Resonant Netting (CRN) is advanced here as a minimal architectural hypothesis for energy-efficient hypothesis selection under the severe communication/computation asymmetry of cortex. Rather than invoking microscopic non-classical coherence or committing to a specific physical substrate, CRN formalizes a two-stage decision loop that is compatible with classical wave media: a transient, low-dissipation pre-selection phase on an active hypothesis graph, followed by a thresholded, metabolically costly fixation and broadcast event. The novelty is threefold. First, we place this architecture within a normative active inference frame, recasting hypothesis selection as a constrained search problem whose energetic cost is dominated by communication events rather than local computation. Second, we provide an open-system formalism (GKSL/Lindblad) for wave transport with operational observables (Liouvillian spectral gap $g(\kappa)$, noise-assisted window width W_κ, and a

maintenance tax) and show in reproducible simulations that an intermediate-noise regime can robustly accelerate convergence on realistic graph topologies. Third, we couple the architecture to a falsifiable energy checkpoint ratio χ that quantifies when wave-layer maintenance remains well below the savings from avoided spikes. Together, these elements situate CRN within mainstream computational neuroscience as a physically explicit, energetically grounded hypothesis about how biological circuits might increase information-per-spike, without overclaiming wall-clock speedups or committing to a specific microscopic ontology.

1. Introduction

1.1 Engineering motivation: why $E_{comm} \gg E_{comp}$ matters for selection/inference

The brain operates under an extraordinarily tight energy budget of roughly tens of watts while performing rapid, high-fidelity hypothesis selection for active inference. A fundamental energy asymmetry constrains this architecture: local neural computation is metabolically inexpensive, whereas long-range communication-spiking and global broadcast-incurs orders of magnitude higher cost. Empirical estimates suggest that communication can consume roughly 35 times more energy than local computation in cortical circuits, making the number of costly communication events a primary metric for selection efficiency.

This energy asymmetry creates an engineering problem: if hypothesis selection were implemented naively—by processing each competing alternative through expensive spike-based global signaling until a winner emerges-the energetic cost would scale linearly with the effective size of hypothesis space, N_{active}, quickly exhausting the brain's budget. Under the Free Energy Principle, the brain must continuously select internal models that best explain sensory data; under these energy constraints, it requires a mechanism to pre-filter competing hypotheses without committing to expensive global signaling for every candidate. CRN (Coherent Resonant Netting) addresses this problem by proposing a two-stage architecture that separates pre-selection in a lower-dissipation regime from final fixation and broadcast.

1.2 Architectural hypothesis: wave pre-selection → thresholded fixation

We propose that the brain implements a hierarchical selection mechanism consisting of two dissociable stages. In the first stage, a transient wave-dynamical episode (modeled as open-system dynamics governed by an effective Hamiltonian on the hypothesis graph, the cognitome) performs efficient pre-selection by redistributing amplitude/probability across competing candidates, leveraging local prediction-error estimates as a biasing potential. This pre-selection regime is quasi-reversible (low-cost) because it operates primarily through interference and phase redistribution before dephasing locks in a result. In the second stage, once a single hypothesis or sparse subset has been sufficiently amplified by the wave episode, an irreversible, thresholded fixation event (captured by a Lindblad sink term in the effective dynamics) triggers a classical spike-based readout and global broadcast for reporting, memory consolidation, and action. The resulting architecture reduces the number of metabolically expensive communication events from $\Omega(N_{active})$ in a classical unstructured search to O(1) per selection act.

Scope clarification. CRN does not rely on microscopic quantum coherence, entanglement, or quantum information processing in neural tissue. It is an architectural and energetic proposal about how a reset-limited, noisy biological circuit could implement hypothesis pre-selection under active-inference constraints. We use the GKSL/Lindblad formalism as a standard open-system model, and the signatures we focus on (spectral gaps, ENAQT-like / noise-assisted transport (NAT) noise windows, and the energy-checkpoint ratio χ defined in

Section 6) are, by construction, compatible with purely classical wave substrates such as coupled oscillators, dendritic wave modes, or photonic reservoirs.

1.3 Claims & Non-claims

To define the scope of the CRN framework precisely, we postulate the following:

Claims:

Architectural claim (H_{wave}): CRN constitutes a two-stage decision circuit combining quasi-reversible wave pre-selection on a hypothesis graph with thresholded classical fixation. This architecture does not require long-lived non-classical coherence and is compatible with classical wave analogs.

Thermodynamic claim (assumption-bound): Under four postulates (Q1–Q4; defined in Section 6.1: O(1) costly events per selection, sparse recruitment $N_{active} \ll N_{total}$, bounded active excitation, and sub-linear scaling of control dissipation), the expected energy per selection satisfies $E_{tax} \ll (N_{active} - 1)E_{comm}$, meaning the wave-layer tax remains well below the spike-communication baseline.

Temporal scope (reset-limited): In biologically typical conditions where reset/refractoriness dominates, CRN does not claim faster wall-clock decisions; the energy advantage derives from reducing the communication event count, not from wall-clock speedup.

Testable signatures (ENAQT-like / noise-assisted transport (NAT)): CRN predicts a non-monotonic dependence of selection efficiency on effective noise/dephasing and robustness characterized by a window width W_{κ}, rather than a fine-tuned point.

Non-claims:

We make no claim of long-lived macroscopic wave coherence in neural tissue (e.g., >1 ms).

We make no claim that non-classical coherence is strictly necessary (classical wave implementations remain plausible).

We make no claim regarding a unique identified substrate, long-term plasticity mechanisms, or unique parameter identifiability from behavior alone.

We make no claims about consciousness, subjective experience, or uniquely quantum mechanisms.

Why has a CRN-like mechanism not become standard in engineered AI systems? First, engineered wave/analog computing and reservoir-style platforms exist (Section 2.3), but they are typically optimized for latency/throughput or hardware convenience rather than for minimizing the count of metabolically costly broadcast-like events per decision. Second, biological circuits operate under a strict power budget and in a reset-limited regime, where the operative constraint is energy-per-act under E_comm ⩾ E_comp, not raw wall-clock speed. Accordingly, CRN is framed as a biologically plausible hypothesis about how inexpensive local analog dynamics could reduce expensive communication events and yield testable dissociations, rather than as a universally superior algorithm for generic machine-learning workloads.

1.4 Roadmap of the paper

The paper unfolds as follows. Section 2 provides information-thermodynamic anchors: the communication-cost dominance and Landauer's principle. Section 3 introduces the CRN architecture, the concept of the cognitome, and the temporal hierarchy. Section 4 formulates the minimal GKSL/Lindblad model with explicit observables (spectral gap, window width). Section 5 demonstrates ENAQT-like / noise-assisted transport (NAT) netting on toy (N=10) and stress-test (N=1000) graphs, confirming the non-monotonic noise optimum. Section 6 derives

the energy-advantage argument under postulates Q1-Q4, formulating the payoff criterion $E_{save} > E_{tax}$. Finally, Section 7 discusses the implications, proposing minimal falsifiable predictions (P1-P6) and dissociation protocols, including a Drosophila anesthetic-perturbation protocol and a mammals/humans extension (Supplementary Note S5.2), while also addressing limitations and positioning CRN relative to prior art.

Table 1 | CRN parameter glossary (operational meanings and example empirical proxies).

Parameter	**Meaning in CRN**	**Empirical proxy (examples)**
γ	Graph coupling / transport strength on the active hypothesis subgraph.	Effective functional connectivity; coupling inferred from dynamics.
κ	Effective dephasing/noise rate interpolating between interference and overdamped diffusion.	Stress/anxiety proxies; anesthetics; temperature; membrane-potential variability.
η	Sink/readout coupling rate capturing Stage-II fixation/commitment (absorption to the sink).	Readout excitability/threshold proxies; ERP/EMG threshold markers.
τ_{trans}	Stage-I transport / pre-selection timescale on the active subgraph.	Subthreshold integration window; LFP/MEG phase-persistence time.
τ_{reset}	Reset/refractory (cooldown) timescale setting the act rate in reset-limited operation.	Inter-decision interval; recovery from synaptic depression; refractory signatures.
χ	Energy checkpoint ratio $\chi = E_{tax} / E_{comm}$ (wave-layer tax per act vs one spike/broadcast event).	Metabolic markers (NADH/FAD, CMRO2/CBF) combined with spike/burst counts per act.
N	Full hypothesis repertoire size (cognitome scale; context for communication-cost dominance).	Model/representational complexity estimates; not directly measured in vivo.
N_{active}	Recruited active hypothesis subgraph size per act.	Task complexity; number of simultaneously engaged features/populations; decoding dimensionality.
W_{κ}	NAT window width: robustness range of κ around κ* (e.g., FWHM on log10 κ).	Width of performance vs κ-proxy curve (behavioral or dynamical marker).

2. Background and Theoretical Framing

2.1 The Normative Frame: Active Inference as a Search Problem

The Free Energy Principle (FEP) provides a normative account of how adaptive agents maintain structural integrity by selecting internal states (hypotheses, beliefs) that minimize variational free energy with respect to sensory data (Friston, 2010). For context, one common decomposition is:

$$F(q,o) \approx D_{KL}(q(s) \| p(s \mid o)) - E_{q(s)}[\ln p(o \mid s)] \quad (1)$$

We use this framing only to motivate hypothesis selection as a constrained search problem; we will not rely on the exact decomposition of F in what follows.

While FEP successfully describes the objective function of the brain, it leaves open the question of physical implementation. Minimizing F over a high-dimensional hypothesis space implies a search process. If this search is performed via iterative, spike-based message passing for every candidate hypothesis, the metabolic cost becomes prohibitive. CRN does not propose an alternative to FEP; rather, it offers a physical mechanism for implementing the initial, coarse-grained phase of free energy minimization (pre-selection) under strict thermodynamic constraints.

2.2 Information-Thermodynamic Anchors: The Cost of Communication

Information processing is physical and therefore costly. Landauer's principle sets the fundamental lower bound for irreversible logical operations (e.g., bit erasure) at k_B T ln 2 ≈ 3 × 10^{-21} J at body temperature (Landauer, 1961). However, biophysical estimates of neural signaling costs (spiking and synaptic transmission) are many orders of magnitude above this bound (Attwell and Laughlin, 2001; Lennie, 2003). The primary energetic driver in the brain is not the logical manipulation of bits (computation), but their physical transport (communication).

Generating and propagating an action potential, restoring ionic gradients, and delivering synaptic output is metabolically expensive (order-of-magnitude estimates are on the scale of ~10^9 ATP molecules per spike), whereas local subthreshold integration in dendrites is relatively inexpensive (Lennie, 2003). This creates a massive energetic asymmetry: $E_{comm} \gg E_{comp}$.

From an engineering perspective, this dictates a clear design rule: "Compute locally, broadcast rarely." A thermodynamically efficient architecture must therefore possess a mechanism to "net out" incompatible hypotheses locally-using low-dissipation transient dynamics-before committing to the expensive, irreversible act of global broadcasting.

2.3 Reference Class and Orthogonal Novelty

CRN belongs to the broader class of wave-based and reservoir computing architectures, which exploit the physics of the substrate for computation. We acknowledge conceptual kinship with Photonic Reservoir Computing (Vandoorne et al., 2014) and Coherent Ising Machines (Yamamoto et al., 2017). Our starting point is the communication-dominant energetics of cortex: formally, $E_{comm}/E_{comp} \gg 1$, where E_{comm} denotes the energetic cost of a costly communication event (spike/burst and associated broadcast) and E_{comp} denotes local subthreshold integration/computation. However, CRN distinguishes itself along three orthogonal axes relevant to neuroscience:

The "Reset-Limited" Regime: Unlike photonic solvers designed for nanosecond speedups, biological circuits are constrained by millisecond-scale refractory periods *($\tau_{reset} \gg \tau_{trans}$).* CRN does not claim to beat the "wall-clock" speed of a single neuron; instead, it maximizes the informational yield per spike, effectively parallelizing the search within the refractory window.

The Energy Checkpoint ($E_{save} > E_{tax}$): We introduce a rigorous falsifiability criterion. The energy saved by avoiding unnecessary spikes must exceed the "metabolic tax" of maintaining the pre-selection wave layer. This moves the discussion from qualitative metaphors to quantitative bioenergetics.

Noise as a Resource (ENAQT-like / noise-assisted transport (NAT)): Unlike classical attractors that require noise suppression, CRN predicts an Environment-Assisted Transport regime. We hypothesize that the "warm and wet" noisy environment of the brain is not a bug but a feature, tuning the dephasing rate κ into an optimal intermediate window that accelerates consensus formation without destroying the signal.

3. CRN Hypothesis: Architecture and Operating Regimes

3.1 The Cognitome and the Active Subgraph (N_{total} vs. N_{active})

At the core of the CRN framework lies the cognitome-a structured, hypergraph representation of the brain's long-term memory, causal models, and semantic relationships (Anokhin, 2021). Formally, we define the cognitome as a graph G = (V, E), where nodes V represent latent hypotheses (e.g., object categories, feature combinations, motor primitives) and edges E encode learned associations.

Crucially, the cognitome is not a flat, unstructured catalog; it is hierarchically organized. However, for thermodynamic analysis, we must distinguish between two scale parameters:

N_{total}: The size of the full cognitome repertoire (potentially 10^6-10^9 nodes).

N_{active}: The effective size of the competing hypothesis space recruited for a single decision act (typically 10^1-10^3 nodes). Throughout, N_{active} refers to the active subgraph over which H_{net} acts during one selection episode.

CRN posits that the energetically expensive pre-selection process operates only on the active subgraph (N_{active}), not the entire brain. The recruitment of this subgraph is context-dependent, but once formed, the problem reduces to selecting the optimal node from N_{active} under energy constraints.

3.2 The Two-Stage Loop: Wave Pre-Selection and Thresholded Fixation

We propose that the decision cycle within the active subgraph is split into two physically distinct stages (see Figure 1):

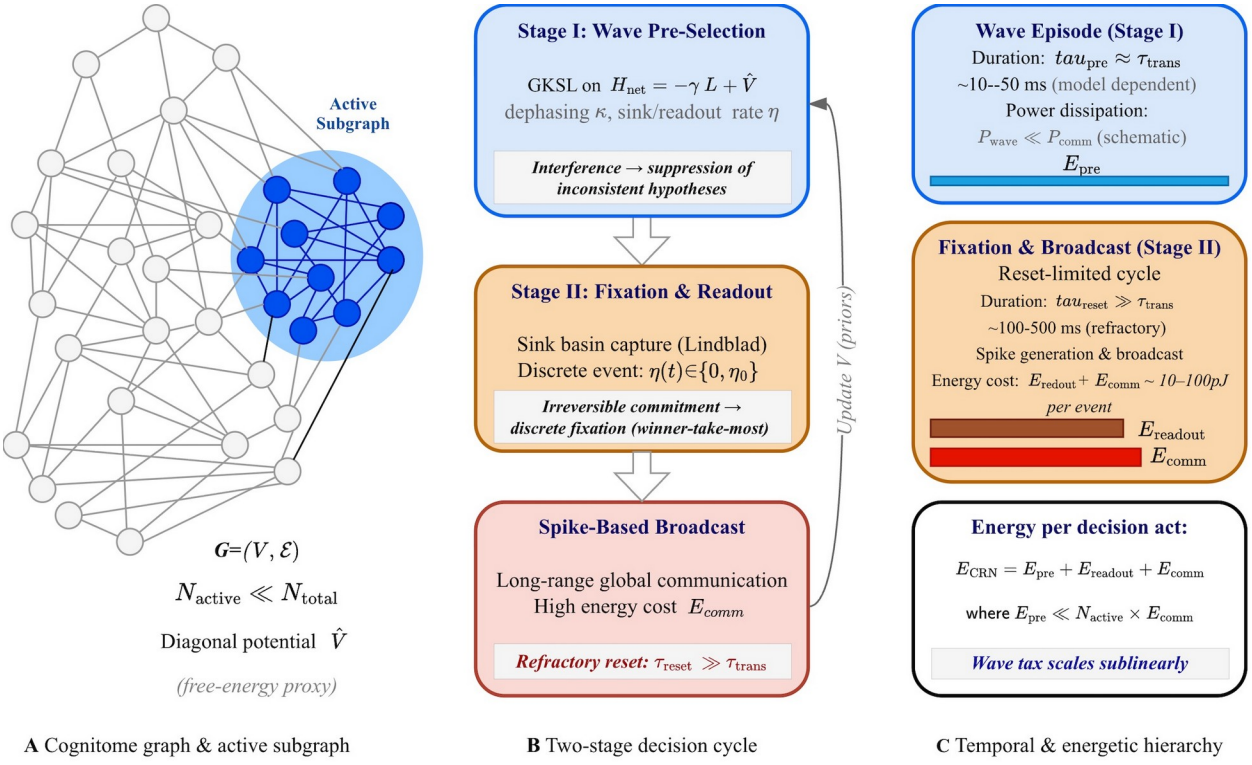

A Cognitome graph & active subgraph **B** Two-stage decision cycle **C** Temporal & energetic hierarchy

Figure 1

Stage I: Wave Pre-Selection (The "Netting" Phase). Before any classical spike is emitted, the active subgraph undergoes a transient, wave-like dynamical episode. This phase is governed by an effective Hamiltonian where

nodes exchange amplitude/phase information. The key mechanism is interference: inconsistent hypotheses (those with contradictory inputs or inhibitory links) cancel each other out via destructive interference, while the "fittest" hypothesis (supported by data and priors) acquires dominant amplitude. This stage is metabolically low-cost because it relies on analog transport rather than digital spiking.

Stage II: Irreversible Fixation (The Readout). Once the wave dynamics converge (or sufficiently amplify a mode), a threshold element triggers rapid capture into a dissipative sink basin. In the GKSL model this is represented by an interaction with a "sink" (in the Lindblad sense), standing for an irreversible commitment to a decision (e.g., a threshold-and-fire/self-quenching event). This fixation triggers the high-cost macroscopic broadcast of a spike or burst, terminates the cycle, and initiates reset.

3.3 Temporal Hierarchy: The "Reset-Limited" Regime

A defining feature of biological neural networks is the timescale of refractoriness. Unlike photonic chips designed for nanosecond throughput, neurons have a mandatory "reset" period (τ_{reset}) lasting milliseconds. CRN operates in a reset-limited regime, defined by the inequality:

$$\tau_{trans} \ll \tau_{reset}$$

where τ_{trans} is the characteristic timescale of the wave-dynamical pre-selection (transport time).

In this regime, the system is not limited by how fast the wave propagates, but by how often it can "fire". The thermodynamic advantage of CRN comes from using the low-dissipation interval τ_{trans} to filter out errors, ensuring that when the expensive time τ_{reset} is finally paid, it is paid for a high-quality decision. We expressly do not claim that CRN accelerates wall-clock reaction times beyond standard physiological limits; rather, it maximizes the informational value per Joule dissipated. The energy bookkeeping and checkpoint logic in Section 6 are formulated explicitly for this reset-limited regime.

3.4 Physical Substrate Agnosticism

While the CRN model is formulated using the GKSL/Lindblad master equation (an open-system formalism), it is substrate-agnostic. The minimal mathematical requirement for 'netting' is not entanglement per se, but the existence of phase memory (τ_{phi}) sufficient to support interference over the timescale of subgraph traversal $(\tau_{phi} \geq \tau_{trans})$.

Candidate implementations that could support such phase memory include (non-exhaustive):

Subthreshold traveling waves and oscillatory modes in dendritic arbors and local circuits.

Endogenous extracellular electric fields enabling ephaptic coupling in densely packed neural tissue (Jefferys, 1995; Anastassiou et al., 2011).

Engineered classical analog platforms used as proof-of-principle substrates for coherent wave computation (Vandoorne et al., 2014; Van der Sande et al., 2017).

The model treats the specific physical vehicle as an implementation detail. If a classical mechanism (e.g., coupled oscillators) can sustain phase relationships long enough to perform interference-based filtering, it satisfies the H_{wave} hypothesis. Thus, CRN remains falsifiable based on its dynamics and spectral signatures, independent of the specific microscopic carrier.

4. Minimal Formal Model and Operational Metrics

4.1 Hypothesis Graph and Effective Hamiltonian

We model the active hypothesis subgraph as a connected, undirected graph G=(V,E) with |V|=N_{active} nodes. The graph structure encodes the semantic and statistical relationships between competing hypotheses (e.g., phonemes in speech recognition or motor primitives).

The dynamics on this graph are governed by an effective Hamiltonian (H_{net}), which drives the unitary (wave-like) part of the evolution:

$$H_{net} = -\gamma L + V \quad (2)$$

where:

L = D - A is the graph Laplacian, acting as the generator of diffusion or "hopping" between logically connected hypotheses. The parameter γ controls the coupling strength (transport speed).

V = diag(V_1, ..., V_N) is the diagonal potential. Each V_i represents the local 'energetic cost' or surprisal of hypothesis i. In the context of Active Inference, V_i serves as a proxy for local variational free energy (prediction error). The dynamics concentrate amplitude on nodes with minimal V_i.

4.2 Open Dynamics: The Lindblad Master Equation

Crucially, the wave layer is not treated as a closed system: it is an open system exposed to noise and coupled to a readout mechanism. We model the evolution of an effective state descriptor $\rho(t)$ with a Gorini–Kossakowski–Sudarshan–Lindblad (GKSL) generator. We treat ρ not as a quantum density matrix of microscopic degrees of freedom, but as a compact state representation for wave-like population dynamics on the hypothesis graph (diagonal elements track hypothesis populations/probabilities; off-diagonal elements parameterize phase relationships/coherence of the wave-like mode). Our use of GKSL is pragmatic: it provides a compact mesoscopic field theory for open wave-like transport on graphs, analogous to using diffusion or hydrodynamic equations as effective descriptions of many-body media. In minimal form:

$$d\rho/dt = -i[H_{net}, \rho] + \kappa D_{deph}[\rho] + \eta D_{sink}[\rho]. \quad (3)$$

Physical interpretation of the state variable ρ (rho)

In the main text, ρ(t) is treated as an effective coherency (mutual-intensity) matrix of mesoscopic population amplitudes on the active hypothesis graph: the diagonal tracks hypothesis “population/intensity”, while off-diagonals summarize phase-coupling that enables interference-like filtering. This is a mesoscopic classical-wave interpretation (not a claim of microscopic quantum coherence); a fuller mapping and calibration context are provided in Supplementary Note S2.

4.3 Operational Metrics: Spectral Gap and Window Width

In CRN, “resonant” is used in an operational (spectral) sense: efficient pre-selection requires a structured mode spectrum with a separation between fast-decaying components and longer-lived coherent transport modes. This mode separation is what makes the Stage I wave episode a selective, low-dissipation filter rather than generic diffusion. Supplementary Note S3 provides the spectral diagnostics and mode-separation criteria used for this interpretation. In particular, we reserve the “resonant” label for regimes where the Liouvillian spectrum exhibits

a separated slow-mode manifold; when this separation is absent and decay rates form a single broad band, the dynamics reduces to generic noise-tuned diffusion and the term “resonant” should be de-emphasized.

ENAQT-like / noise-assisted transport (NAT) Window Width (W_κ): The CRN hypothesis predicts that transport efficiency (and thus the gap g) is non-monotonic with respect to noise κ. We define the robustness window as a log-range, $W_\kappa = \log10(\kappa_{hi}/\kappa_{lo})$, where κ_{lo} and κ_{hi} are the bounds for which decision efficiency remains above half of its peak value (FWHM on a log10 κ axis). A wide W_κ (order-unity in decades) indicates that the system does not require fine-tuned parameters to operate.

4.4 Time Calibration and Feasibility Checkpoint

The model operates in dimensionless units. To map these to biological reality, we introduce a Feasibility Checkpoint (see Supplementary Note S2 for calibration tables). For a physical substrate to support CRN, its intrinsic phase-memory time τ_{phi} must be comparable to, or exceed, the transport time across the active subgraph: $\tau_{phi} \gtrsim \tau_{trans}$. If a proposed substrate (e.g., purely ionic diffusion) has τ_{phi} orders of magnitude shorter than the required networking time, it is falsified as a candidate for the wave layer. This 'phase-budget' check allows us to filter candidate implementations without committing to a single one in the main theory.

5. Computational Evidence: Noise-Assisted Transport (ENAQT-like / noise-assisted transport (NAT)) and Robustness

5.1 Phenomenology of Netting: the ENAQT-like / noise-assisted transport (NAT) window

The central computational claim of the CRN hypothesis is that efficient hypothesis selection is non-monotonic with respect to noise. Specifically, we predict an ENAQT-like / noise-assisted transport (NAT) regime where intermediate dephasing enhances transport to the readout sink relative to both the coherent ($\to 0$) and overdamped/Zeno-like ($\to \infty$) limits.

We verify this on a minimal hypothesis graph (linear chain, N=10) utilizing the Hamiltonian and Lindblad dynamics defined in Section 4. Figure 2 plots the Liouvillian spectral gap g(κ) as a function of the dephasing rate κ at fixed connectivity γ=4.0 and sink rate η=0.8. The curve reveals three distinct regimes:

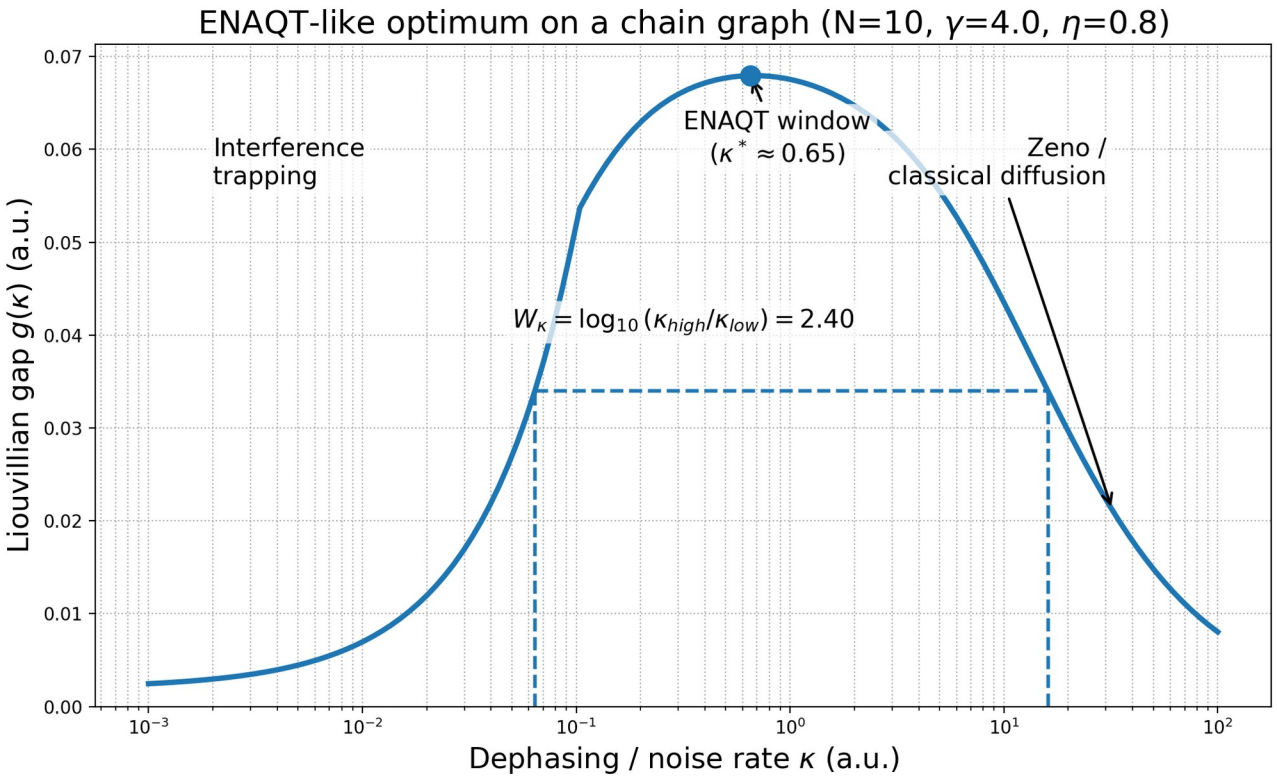

Figure 2

Interference Trapping ($\kappa \approx 0$): In the absence of noise, destructive interference leads to coherent trapping (Anderson-like localization), preventing efficient transport to the sink and yielding a small Liouvillian gap (slow convergence).

The ENAQT-like / noise-assisted transport (NAT) Window (Intermediate κ): As dephasing increases, it suppresses destructive interference of long loops while preserving local coherence. This produces a pronounced maximum of the Liouvillian spectral gap g(κ) at κ=κ*, corresponding to faster convergence to the readout sink.

The Zeno / Diffusive Regime ($\kappa \gg \gamma$): At high dephasing rates, the system becomes overdamped and effectively classical. A Zeno-like suppression freezes coherent spreading, causing decision times to grow and the gap to decrease again (g $\rightarrow$ 0 as κ grows).

Operational interpretation. The gap g(κ) provides a spectral marker of convergence/decision timescales (larger g implies faster approach to the absorbing sink). Robustness is quantified by W_κ (Section 4.3); across the reported sweeps W_κ is order-unity in log10 κ, supporting the claim that the mechanism is not fine-tuned.

5.2 Scaling to Cortical Subgraph Sizes (N=1000)

A critical question is whether this resonant advantage persists in high-dimensional hypothesis spaces typical of cortical active subgraphs. To address this, we subjected the model to a "stress test" on a Watts-Strogatz small-world network (Watts and Strogatz, 1998) with N=1000 nodes (see Figure 3).

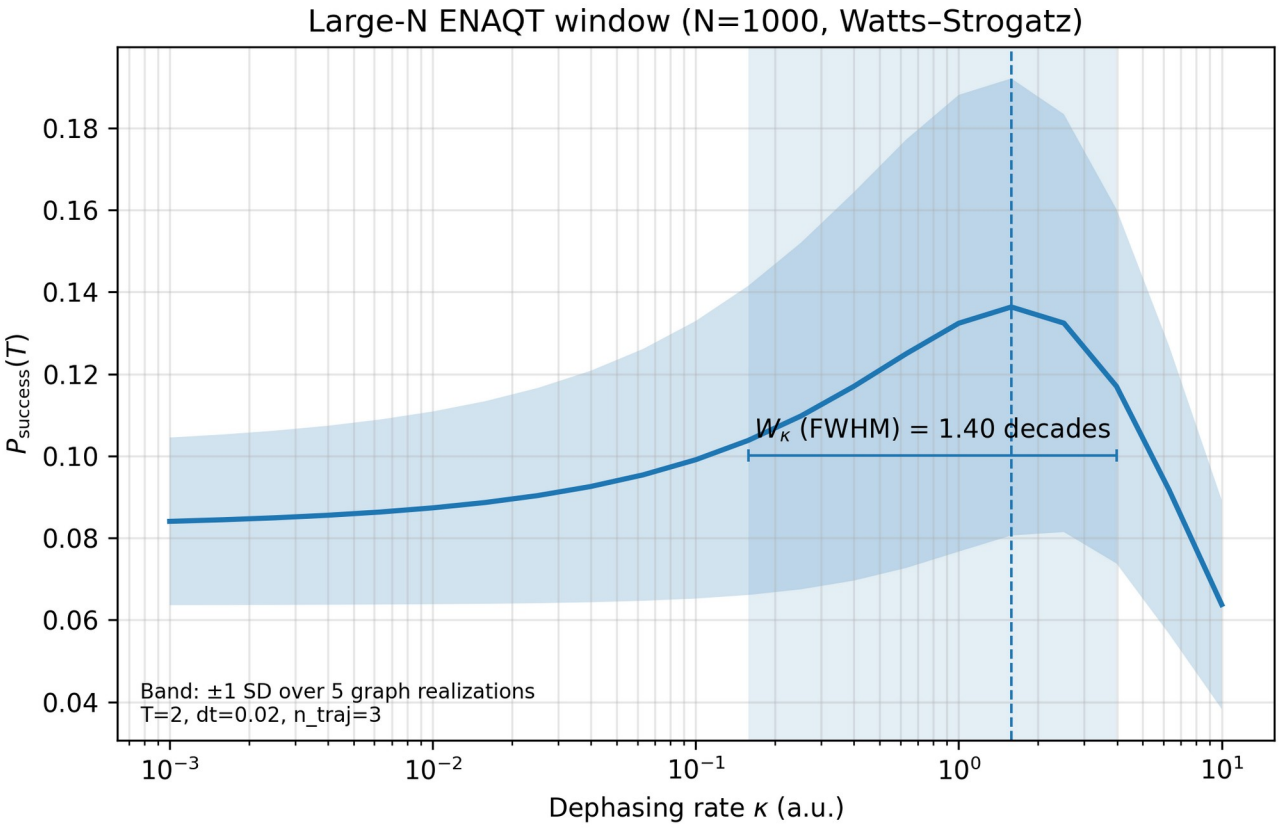

Figure 3

Despite the two orders of magnitude increase in system size, the ENAQT-like / noise-assisted transport (NAT) signature remains robust. Figure 3 shows the finite-horizon success probability $P_{success}(T)$ as a function of the effective dephasing/noise rate κ, averaged over multiple Watts–Strogatz realizations. The curve is non-monotonic with a well-defined maximum at $\kappa=\kappa^*$, and the near-optimal region is broad: the window width W_κ (FWHM on a log10 κ axis) remains order-unity in decades. This supports the claim that the resonant regime is not a fragile fine-tuned point and can persist in high-dimensional active subgraphs with small-world structure.

Topology robustness. To probe sensitivity to coarse graph structure, we compare normalized spectral-gap curves across several graph families. When plotting $g(\kappa)/g(\kappa^*)$ versus κ/κ^* for chain, Watts–Strogatz, and modular graphs (γ=4.0, η=0.8), the curves largely collapse (Figure 4), indicating that the ENAQT-like / noise-assisted transport (NAT) marker is compatible with multiple plausible circuit/connectome motifs.

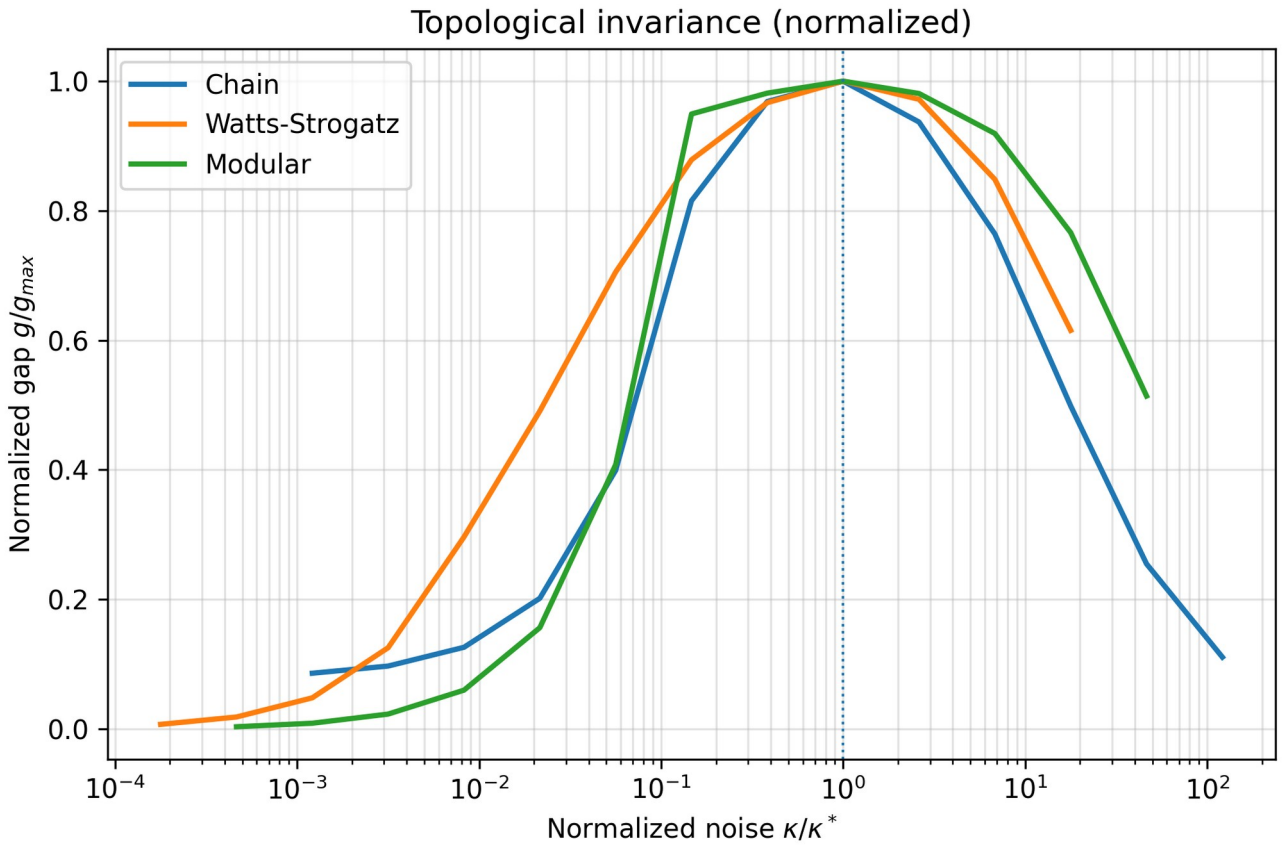

Figure 4

5.3 Robustness to Readout Nonlinearity

The minimal model assumes a linear sink operator (D_{sink}). However, biological readouts likely involve thresholding (e.g., a neuron firing only after membrane potential crosses a limit). We relaxed the linearity assumption by introducing a non-linear sink rate $\eta(I)$ that activates only when the population at the target node exceeds a threshold P_{th}.

Numerical simulations confirm that the ENAQT-like / noise-assisted transport (NAT) peak persists under thresholded conditions. While the absolute time-to-decision increases slightly due to the accumulation requirement, the relative advantage of the optimal noise regime over the ballistic and diffusive limits is preserved. This suggests that the "netting" mechanism is a generic property of open wave dynamics on graphs, not an artifact of a specific linear operator.

Figure 5 illustrates this point on the large-N proxy: at a representative intermediate-noise setting (κ=1.0), the time course of $P_{success}$(t) remains comparable under a thresholded sink, with a delayed but still monotonic rise once the thresholded readout activates.

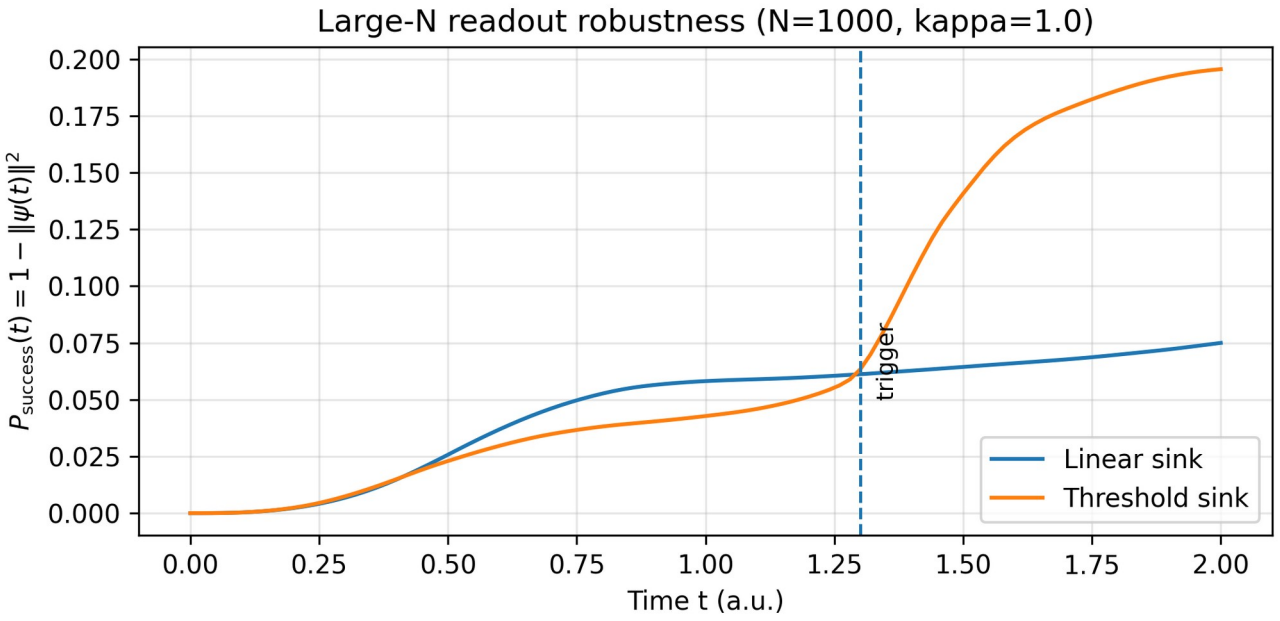

Figure 5

5.4 Reproducibility

To ensure rigor and transparency, the results presented in this section are fully reproducible using the R12-CROWN Simulation Suite. The complete codebase, including the GKSL solver, graph generators, and scripts to reproduce the core figures (including the N=1000 stress test), is archived on Zenodo (concept DOI: 10.5281/zenodo.18338260; version used here: 10.5281/zenodo.18338261). The suite includes an automated validation report verifying that the qualitative ENAQT-like / noise-assisted transport (NAT) signatures (spectral gap peak and $\chi > 0$) hold across the tested parameter ranges.

6. Energy advantage argument and checkpoints (assumption-bound)

6.1 Postulates Q1-Q4 and scope of the claim

The energy advantage claim in CRN is not presented as a universal law. It is conditional on four explicit postulates that can, in principle, be operationalized in simulations and experiments on candidate substrates and circuits.

Q1 (communication-dominant baseline). The dominant energetic cost of a selection act in the classical baseline is proportional to the number of metabolically costly communication events (spike/burst emission and broadcast).

Q2 (O(1) fixation/broadcast events). In CRN, the architecture is arranged such that the irreversible readout/fixation and subsequent broadcast occur a small constant number of times per act (ideally one winner), independent of N_{active}.

Q3 (bounded active excitation during pre-selection). The wave episode does not recruit O(N_{active}) high-amplitude, spike-like events. Instead, it operates in a passive/subthreshold regime where cumulative active dissipation during the pre-selection window remains bounded or sublinear in N_{active}.

Q4 (sublinear scaling of maintenance/control losses). The wave-layer maintenance and control power P_{tax} does not grow linearly with N_{active} over the relevant operating range; otherwise the tax cancels any savings.

In this article, CRN is advanced as an architectural hypothesis (H_{wave}) plus an assumption-bound thermodynamic criterion. We do not claim a generic wall-clock speedup in the biologically typical reset-limited regime $(\tau_{reset} \gg \tau_{trans})$.

6.2 Classical baseline: lower bound for burst-gated selection

Define a selection scheme as burst-gated if each of the N_{active} competing hypotheses can influence the global winner within one act only by emitting at least one costly communication event (a burst/spike-equivalent broadcast).

In an unstructured needle-in-a-haystack task (exactly one hypothesis is correct), any burst-gated scheme that returns the correct index with constant success probability requires $\Omega(N_{active})$ costly events per act. Proof sketch: if, on average, Q hypotheses emit a costly event and are therefore 'examined', then with a uniformly random target the success probability is at most Q/N_{active}; achieving constant success implies $Q=\Omega(N_{active})$.

This lower bound is independent of the physical details of the classical circuit. It is an energetic statement: when E_{comm} is large, paying for $O(N_{active})$ costly events is prohibitive in the communication-dominant regime.

6.3 Break-even inequality, energy checkpoint, and measurement strategy

CRN changes the cost structure by separating (i) a wave-like pre-selection episode and (ii) a discrete readout/fixation/broadcast event.

Operationally, we parameterize the wave-layer tax per decision act as:

$E_{tax} = P_{tax} / f_{fix}$, with (reset-limited) $f_{fix} \approx 1/\tau_{reset}$. (4)

where P_{tax} is the mean additional power required to maintain and control the wave layer while it is capable of executing the Stage I episode, and f_{fix} is the mean act rate (inverse mean cycle time).

$E_{save} > E_{tax}$, with $E_{save} \approx (N_{active} - 1)\cdot E_{comm}$. (5)

A convenient dimensionless checkpoint is the ratio $\chi := E_{tax}/E_{comm}$. (6)

Here χ denotes the energy-checkpoint ratio; the open-system state descriptor in Section 4 is written as $\rho(t)$.

For CRN to have a clear energetic advantage in the communication-dominant regime, χ should satisfy $\chi \lesssim 10^{-2}$ (wave layer tax at most a few percent of one spike-equivalent event), with $\chi \gtrsim 10^{-1}$ treated as a red-line region where the putative advantage effectively disappears and the classical baseline may be competitive.

In practice, empirical or model-based estimates of P_{tax} and f_{fix} (to bound E_{tax}) and of E_{comm} must be precise enough to place χ relative to this safe/red-line band. Supplementary Note S4 provides template sweeps and payoff maps for χ across control parameters (e.g., κ, γ, topology), given these estimates. Figure 6 provides an illustrative sweep of χ as κ varies at fixed γ and η.

Illustrative order-of-magnitude example (heuristic). If the wave layer is instantiated as transient dendritic field dynamics in a small L5 microcolumn (≈100 neurons), the incremental maintenance power P_tax can be approximated by the energetic overhead of sustaining subthreshold dendritic currents/oscillatory synchrony during the pre-selection interval. The corresponding per-act tax is E_tax = P_tax/f_fix (reset-limited f_fix ≈

1/τ_reset). If this per-act overhead is on the order of only a few percent of one spike-equivalent broadcast event E_comm (e.g., E_tax ≈ 0.02-0.05·E_comm), then χ = E_tax/E_comm falls below the red-line and into the intermediate band (χ ~0.02-0.05). This is an illustrative heuristic rather than a substrate commitment; its role is to make χ empirically legible and falsifiable. A practical indirect marker for Q4/χ is scaling: as task complexity increases (larger N_active), the incremental metabolic response attributable to the pre-selection regime (e.g., NADH/FAD fluorescence, CBF/CMRO2) should grow sublinearly relative to behavioral throughput; an approximately linear growth would indicate violation of Q4 or drift into the red-line χ regime.

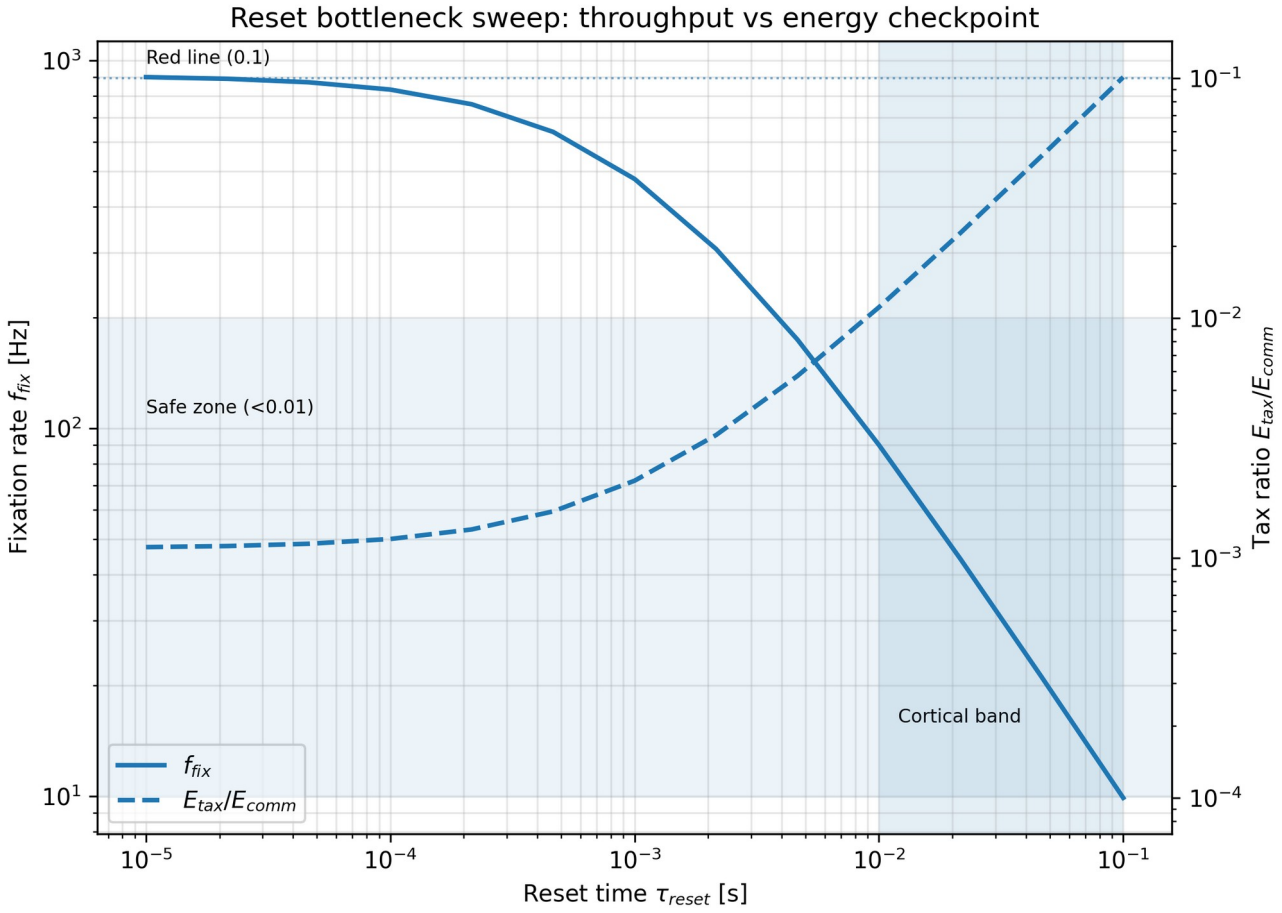

Figure 6

Measurement strategy (operational, not substrate-specific). For a submission-level presentation, χ can be bounded and reported via the following minimal steps (details and worked templates: Supplementary Note S4).

1. Define the selection act and measure the act rate f_fix (≈ 1/τ_reset), verifying the reset-limited regime (τ_reset ⩾ τ_trans).
2. Estimate E_comm (energy of one spike/burst/broadcast event) from spike/burst counts per act together with metabolic proxies (order-of-magnitude bounds suffice).
3. Estimate the incremental wave-layer maintenance/control power P_tax and its scaling with task complexity (N_active) as an indirect Q4 check; compute the per-act tax E_tax = P_tax / f_fix.
4. Compute χ = E_tax / E_comm and classify it relative to the safe band (χ ≲ 0.01) versus the practical red-line (χ ≳ 0.1), reporting conservative uncertainty.

6.4 Falsifiability checkpoint

The thermodynamic advantage component of CRN is falsified if empirical or model-based accounting yields E_{tax} comparable to, or exceeding, the communication baseline savings, i.e., if $\chi/(N_{active} - 1)$ is not clearly below unity for plausible N_{active}. Separately, if the wave-like pre-selection cannot be made to operate without recruiting $O(N_{active})$ spike-like events (violating Q3) or if maintenance/control losses scale approximately linearly with N_{active} (violating Q4), then the advantage collapses even if an ENAQT-like / noise-assisted transport (NAT) optimum exists.

Therefore, CRN deliberately couples its architectural proposal to an explicit 'energy checkpoint': the claim is not that wave dynamics are exotic, but that they can reduce the count of expensive communication events without paying an even larger hidden tax.

7. Discussion: Falsifiability, Positioning, and Conclusion

Scope reminder. Throughout this Discussion we adhere to the scope control summarized in the Claims & Non-claims block (Section 1.3), in particular the reset-limited temporal scope and the assumption-bound nature of the energy argument.

Interpretational scope (tool vs ontology). It is critical to distinguish the mathematical formalism employed here from ontological claims about the brain. By utilizing the GKSL equation, we adopt a tool from open-system physics to model mesoscopic coherent wave dynamics, analogous to its use in classical optics and hydrodynamics.

We explicitly do not postulate that the brain maintains macroscopic quantum coherence (e.g., in microtubules) at physiological temperatures. Instead, “coherence” in the CRN context refers to transient phase-locking of neural population codes. The phenomena we report—interference trapping (Anderson-like localization) and ENAQT-like / noise-assisted transport (NAT)—are generic properties of wave systems in disordered media and do not require non-classical states of matter.

7.1 Minimal Falsifiable Predictions (P1-P6)

The utility of the CRN framework rests on its vulnerability to falsification. We derive six specific experimental signatures that distinguish the CRN mechanism from generic classical diffusion or random search models.

P1: Non-monotonic noise dependence with a spectral ENAQT-like / noise-assisted transport (NAT) marker. Efficiency of hypothesis selection (e.g., reaction time, accuracy, or convergence time to fixation) should peak at an intermediate effective noise/dephasing level. Critically, the behavioral optimum should track a phase-sensitive spectral marker of the wave layer: in the minimal model this is the Liouvillian spectral gap $g(\kappa)$, whose maximum corresponds to the fastest relaxation rate. Falsification: (i) monotonic improvement as noise is reduced, or (ii) a purely behavioral non-monotonicity explainable by generic stochastic resonance, without a corresponding maximum/shift in the spectral marker (or an equivalent phase-sensitive relaxation proxy).

P2: Robustness window (W_κ). The intermediate-noise regime should not be a fine-tuned point; a near-optimal window should persist over an O(1) relative range of κ. Operationally, we summarize robustness by the window-width metric W_κ (half-maximum width on a log κ axis; Section 5). A biologically plausible regime corresponds to $\Delta\kappa/\kappa_{opt} \gtrsim 0.5\text{-}1$ (equivalently $W_\kappa \gtrsim 0.3\text{-}1$ decades). Falsification: an ultra-narrow peak with $\Delta\kappa/\kappa_{opt} \ll 0.1$ ($W_\kappa \ll 0.1$ decades), implying fragile tuning.

P3: Dissociation of reset and noise. Perturbations that act primarily on the classical fixation/reset layer (τ_{reset}) should scale the maximum act throughput and shift overall latency roughly proportionally, while leaving the

location of the ENAQT-like / noise-assisted transport (NAT) optimum in κ largely unchanged. Perturbations that act primarily on wave-layer noise/dephasing κ should reshape the κ-dependence (including κ_{opt} and W_κ) and, where measurable, the spectral gap $g(\kappa)$, without producing the same throughput-limited scaling. Falsification: reset-like and noise-like manipulations produce indistinguishable effects, i.e., the same changes in throughput and the same κ-optimum/curve shape.

P4: Energy checkpoint as a dimensionless red-line. As derived in Section 6, the relevant viability quantity is the dimensionless ratio $\chi := E_{tax}/E_{comm}$, where $E_{tax} = P_{tax}/f_{fix}$ is the per-act wave-layer tax and E_{comm} is the energy of one spike-equivalent costly communication event. CRN's claimed energetic advantage requires $\chi \ll 1$; we treat $\chi \gtrsim 0.1$ as a practical red-line/forbidden region where the wave layer becomes thermodynamically disadvantageous. Falsification: empirical estimates of P_{tax} and f_{fix} placing χ in or above this red-line band under realistic operating conditions (with $P_{tax} \cdot \tau_{decision}$ as one estimator of E_{tax} when $\tau_{decision} \approx 1/f_{fix}$ in the reset-limited regime).

P5: Spectral and functional shifts under anesthesia. If general anesthetics perturb the wave layer primarily by increasing effective dephasing/noise or weakening effective coupling, they should move the system away from the intermediate-noise optimum. Operationally, anesthesia should be accompanied by predictable shifts in (i) the inferred *κ-optimum/window* (from behavior) and, where accessible, (ii) relaxation-rate/spectral proxies consistent with a change in *$g(\kappa)$*. Falsification: robust anesthetic effects on the behavioral endpoint with no measurable shift in these noise-optimum markers (or an opposite-direction shift inconsistent with the ENAQT-like / noise-assisted transport (NAT) mechanism).

P6: Human/mammalian extension (two-stage dissociation). In mammalian/human decision tasks, putative Stage I pre-selection markers (e.g., beta/gamma-band LFP coherence or phase-locking within PFC and frontoparietal networks) should exhibit a non-monotonic dependence on a noise-proxy κ (stress/anxiety level, pharmacological perturbations, or controlled sensory noise), with an intermediate optimum. In contrast, Stage II fixation/commitment markers (e.g., P300 latency/amplitude shifts, ERP/EMG threshold markers of motor commitment) should degrade predominantly monotonically as κ increases. This dissociation is an architectural prediction of the two-stage CRN loop rather than a claim about any single microscopic substrate. Operationally, κ can be proxied by within-subject manipulations of arousal/stress or mild anesthetic/neuromodulatory dose at fixed task demands, while fixation can be proxied by threshold-crossing latencies or the onset of stereotyped commitment signatures (e.g., P300, LRP/EMG onset).

7.2 Proposed Validation Protocol: The Drosophila Model

To test predictions P1-P3 and P5 (and to estimate the window width W_κ from the κ-latency curve), we propose a validation protocol using Drosophila melanogaster, a model organism offering genetic access to ion channels and tractable decision circuits (see Supplementary Note S5 for the detailed protocol). As one concrete handle on reset dynamics, temperature-sensitive shibire (shi^{ts1}) manipulations can reversibly disrupt synaptic vesicle recycling in targeted circuits, effectively altering recovery/reset timescales (Kitamoto, 2001). The dissociation logic is summarized in Figure 7. A conceptual sketch of an optional high-resolution "fine-structure" search (localized resonance windows superimposed on an Arrhenius/Q10-like trend) is shown in Figure 8.

The core logic involves a 2 x 2 dissociation design:

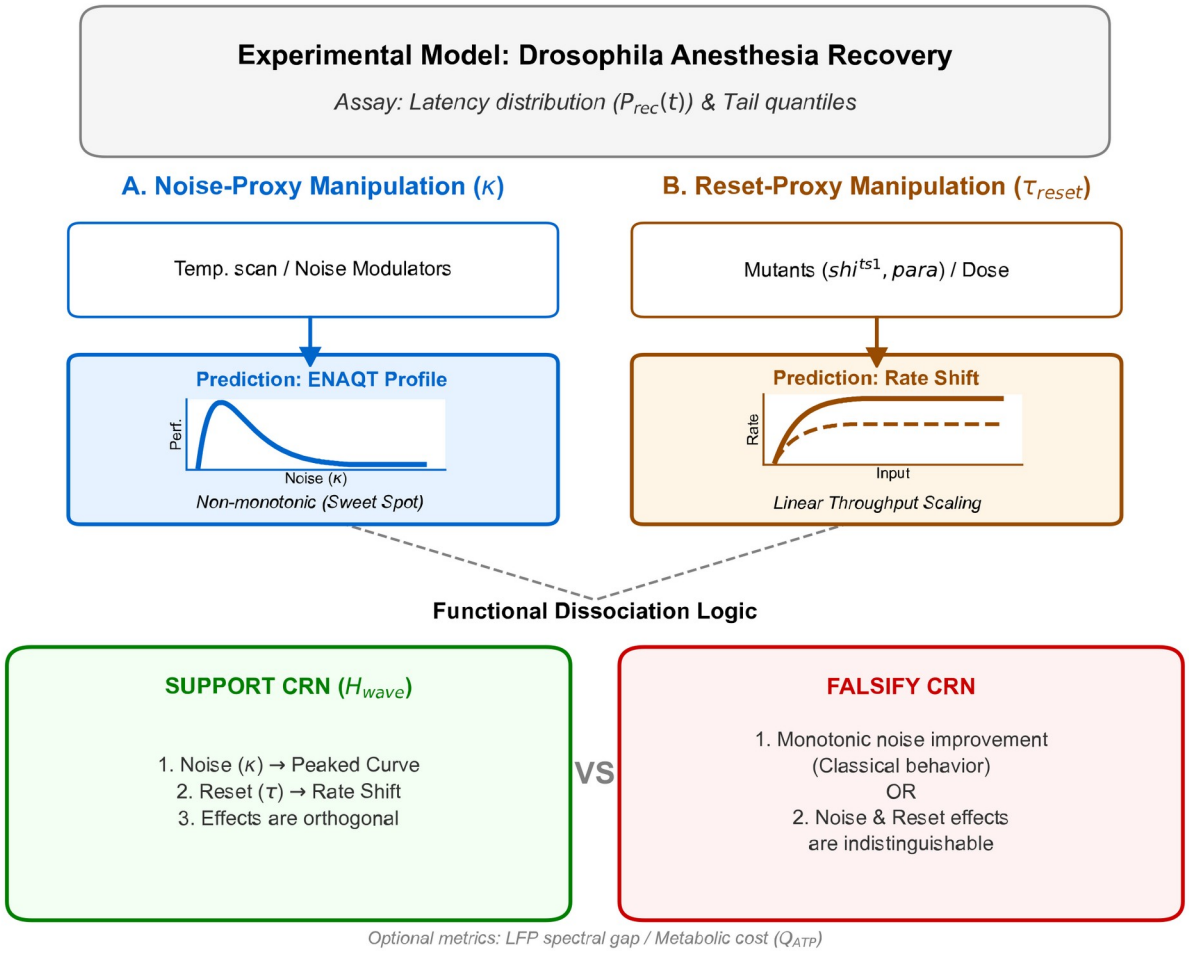

Figure 7

Manipulate Noise *(κ):* Using temperature modulation or pharmacology (e.g., sub-anesthetic isoflurane) to alter channel fluctuation rates.

Manipulate Reset *(τ_{reset}):* Using mutants (e.g., para or Shaker) with altered refractory periods.

Expected Outcome: CRN predicts that manipulating κ will trace the non-monotonic ENAQT-like / noise-assisted transport (NAT) curve for decision latency, while manipulating τ_reset will approximately rescale throughput via f_fix ≈ 1/τ_reset. Together, this dissociates noise-driven netting effects from reset-limited fixation dynamics.

In the same dataset, the *κ-latency* curve provides an empirical estimate of the functional window width W_κ (e.g., half-maximum width around κ_{opt}), directly addressing P2. Overall, this protocol primarily targets P1-P3 and P5; P4 requires complementary metabolic/energetic estimates (Section 6).

Strong (optional) signature: fine-structure resonance windows. Beyond the minimal ENAQT-like / noise-assisted transport (NAT) non-monotonic dependence on a noise proxy κ, CRN suggests that sufficiently high-resolution scans over temperature (or other noise proxies) may reveal localized "resonance windows"—narrow bands where recovery speed (e.g., 1/τ_reset from the recovery-time distribution) deviates sharply from an otherwise smooth Arrhenius/Q10-like baseline (Figure 8). We treat this as a high-resolution, supportive marker rather than

a required success criterion: heterogeneity and coarse sampling can wash out narrow windows, so failure to observe fine structure in initial experiments does not falsify the minimal predictions P1–P3/P5.

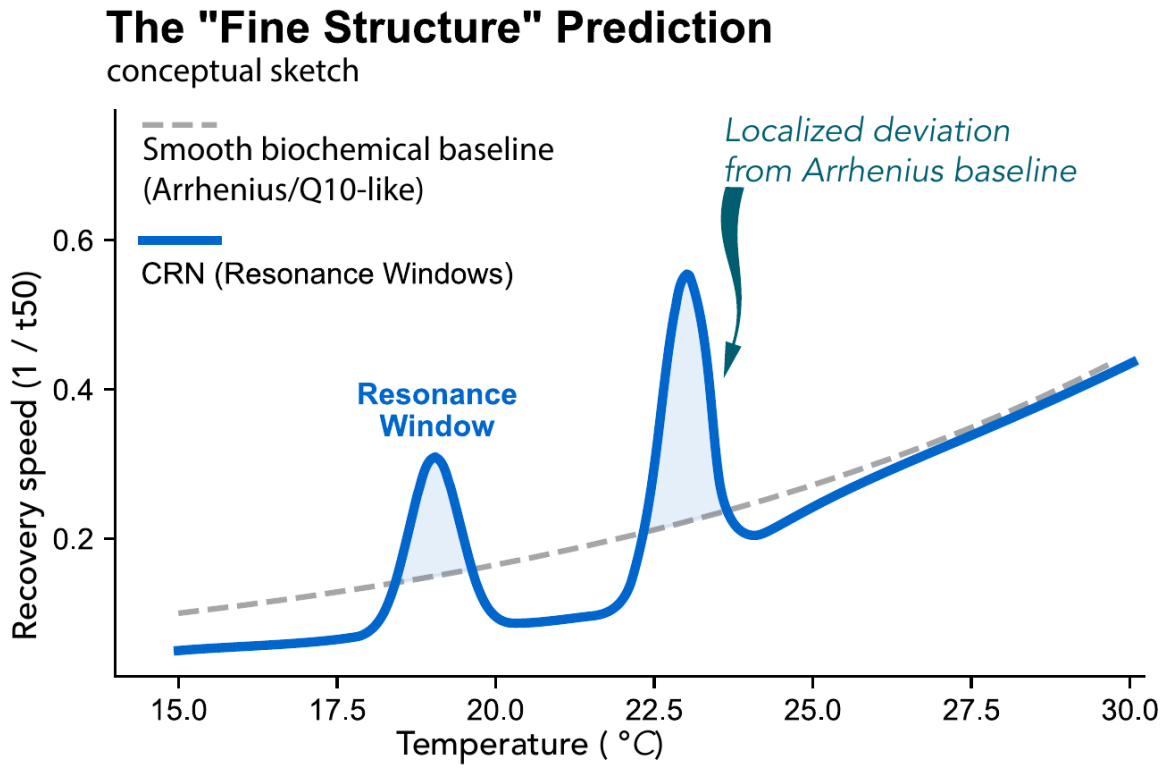

Figure 8

7.3 Biological Implementation and Distinction from Classical Models

A recurrent concern (raised in external critique and anticipated in Section 7.4) is that CRN risks remaining a "beautiful mathematical metaphor" unless it is (i) grounded in plausible neural microcircuit mechanisms and (ii) clearly distinguished from purely classical decision models that can also exhibit intermediate-noise optima. The purpose of this subsection is therefore not to narrow CRN to a single substrate, but to provide one concrete, neurobiologically motivated instantiation and to clarify what aspects of CRN remain distinctive even under classical-wave mimicry.

Biological grounding (candidate substrates). The CRN framework requires a substrate capable of supporting mesoscopic phase/amplitude variables and interference effects on timescales of roughly 10–100 ms. Three biologically plausible candidates are:

- Dendritic integration fields: the electrotonic structure of dendritic arbors supports subthreshold superposition of inputs where relative timing (phase) shapes output amplitude, implementing analog interference before somatic integration.
- Gamma-band synchronization: in "communication through coherence" accounts, effective connectivity is modulated by the relative phase of local gamma oscillations; under this view, ρ_{jk} corresponds to a synchronization (phase-coupling) index between populations/columns.
- Neural field modes: at a mean-field level, propagation of cortical activity can be described by damped wave equations (e.g., Wilson–Cowan with delays). CRN abstracts such continuous fields into a graph representation in which H captures effective connectivity of the relevant modes.

Distinction from attractor and diffusive models (why interference matters). CRN differs from standard attractor networks and random-walk diffusion models in its use of phase-sensitive interference as a passive pruning stage before amplification:

- Vs. attractors: attractor networks (e.g., Hopfield/Wang-style) rely on positive-feedback amplification of firing rates to select a winner, which is metabolically costly and tends to commit to the nearest local minimum. CRN uses destructive interference to prune inconsistent hypotheses before irreversible fixation.
- Vs. diffusion: in an incoherent random walk, probabilities sum additively (Ptotal = P1 + P2). In CRN's wave layer, complex amplitudes sum (Atotal = A1 + A2), allowing cancellation ($|A1 + A2|2 < |A1|2 + |A2|2$) and enabling suppression of inconsistent paths that would remain in a purely diffusive search. Furthermore, as demonstrated in Supplementary Figure S6-2, this interference-based transport can traverse high-energy (high-V) barriers in the hypothesis landscape markedly faster than a classical thermal walk, provided the system operates within the intermediate-noise ENAQT-like / noise-assisted transport (NAT) window.

From abstract graph dynamics to microcircuits (what must be implemented). Independent of substrate, the CRN architecture requires three functional elements: (1) a transient, approximately linear wave-like propagation over a structured hypothesis space; (2) a noise/dephasing mechanism that is tunable (or at least variable) and can place the system in an intermediate-noise ENAQT-like / noise-assisted transport (NAT) regime; and (3) a discrete thresholded readout that converts a distributed pre-selection state into a committed, broadcastable classical outcome. A plausible biological implementation should therefore be evaluated against this triad, rather than against the word "quantum".

Candidate implementations beyond a single-neuron picture. While L5 dendrites provide a convenient concrete mapping, CRN does not require that the entire wave layer resides within one neuron. Two additional implementation motifs are consistent with known neurobiology and preserve the thermodynamic logic $E_{comm} \gg E_{comp}$.

(a) Gap-junction and ephaptic micro-networks as a mesoscopic wave medium. Dense local coupling via gap junctions and ephaptic interactions can support fast, spatially extended subthreshold dynamics without requiring spikes for every participating element. Ephaptic coupling has been demonstrated as a non-synaptic interaction mechanism in cortical tissue, where extracellular fields contribute to coupling between nearby neurons (Anastassiou et al., 2011; Jefferys, 1995). In CRN terms, such coupling can contribute to the effective Laplacian term ($-\gamma L$) that mediates propagation on an active subgraph, while synaptic bombardment and channel noise naturally contribute to effective dephasing κ.

(b) Glia-assisted regulation as a control channel (κ and γ proxies). Even if the wave layer is realized in neuronal membranes/dendrites, control of its operating regime plausibly involves non-neuronal mechanisms (e.g., ionic homeostasis, neuromodulation, and local metabolic support). This matters for CRN because the key experimental lever is not "observe coherence" but "perturb the effective κ/γ regime". A biologically realistic discussion should therefore expect that κ_{eff} and γ_{eff} are composite effective parameters controlled by multiple slow variables, which aligns with our emphasis on regime inference (P1–P3) over point identification.

Interface to fixation/broadcast (why threshold matters). A reviewer-facing weakness of many wave-based proposals is the lack of a credible interface to classical, spike-based computation. CRN's interface requirement is explicit: the readout must implement an irreversible, thresholded conversion from a graded wave-layer state to a discrete classical state that can be maintained and broadcast. In the dendritic mapping, this corresponds to burst initiation mechanisms (e.g., BAC firing) that produce a stereotyped spike packet once apical drive and basal input coincide (Larkum, 2013). In a small-network mapping, it corresponds to a local "ignition" element that flips into a high-activity attractor and engages long-range axonal transmission. This is precisely why we treat the

sink term as a self-quenching threshold element rather than an observer: the architecture requires a physical nonlinearity that enforces discreteness.

What is distinct relative to classical stochastic resonance. A generic non-monotonic dependence of behavioral performance on noise can arise in many classical systems (including threshold devices exhibiting stochastic resonance). CRN's claim is narrower and therefore more testable: the relevant optimum is tied to a phase-sensitive transport transient over a structured hypothesis graph, and it should be trackable by a relaxation-rate proxy, not only by endpoint accuracy/latency. In the formal model, this proxy is the Liouvillian gap $g(\kappa)$, which controls correlation/relaxation time. Translating this to physiology suggests an additional class of observables beyond behavior: the timescale at which population activity (or a dendritic voltage field proxy) relaxes after brief perturbations should itself show a non-monotonic dependence on the κ-proxy, and its optimum should align (approximately) with the behavioral optimum. A mismatch (e.g., a behavioral optimum without any corresponding change in relaxation/correlation time) would weaken the specific CRN mechanism and favor simpler threshold-noise explanations, including classical stochastic resonance in single-threshold devices that do not implement interference-based pruning on a structured hypothesis graph.

Controls against "classical mimicry" (what we can actually demand). Because CRN is explicitly compatible with classical wave analogs, the key scientific objective for the FCN submission is not to prove quantumness (H_{quant}), but to distinguish the architectural H_{wave} claim from purely dissipative attractor competition and from trivial stochastic resonance. Two practical controls are therefore recommended.

First, dissociation controls: noise-proxy versus reset-proxy manipulations should have separable effects, as formalized in P5 and Figure 7. If all manipulations collapse to one scalar "slowing down" factor (i.e., identical changes in throughput, curve shape, and optimum location), the two-stage architecture is not supported.

Second, model controls: in parallel with the Drosophila experiment, fit classical competitor models to the same data class (e.g., a drift-diffusion model with temperature-dependent diffusion and threshold, or a classical coupled-oscillator/reservoir surrogate tuned to match smooth Arrhenius-like dependencies). The goal is not to "win a fit" with more parameters, but to test whether a classical model can reproduce (i) a stable intermediate-noise optimum with finite width W_{κ}, (ii) systematic shifts of κ^* under connectivity-like perturbations, and (iii) the reset/noise dissociation pattern. If it can, the result still supports the existence of a wave-like pre-selection layer (H_{wave}) but weakens any claim of uniqueness; if it cannot, the experiment becomes more discriminative.

As a minimal transport baseline, Supplementary Note S6 provides a direct CRN-versus-CRW comparison on the same toy graph. It highlights an interference-trapping plateau in the coherent limit ($\kappa \to 0$) that is absent in a classical random walk, and its release in the ENAQT-like / noise-assisted transport (NAT) regime (reproducible via R12-CROWN: compare_baselines.py).

Why this helps reviewers. These additions are intended to make the proposal legible to a computational neuroscience audience: (i) they specify what must be implemented biologically (three functional elements), (ii) they acknowledge classical mimicry while making the target of inference explicit (H_{wave} rather than H_{quant}), and (iii) they propose concrete controls that can falsify the two-stage architecture even if an intermediate-noise optimum is observed. This is the pragmatic standard for a Hypothesis and Theory contribution in FCN: a mechanism that is physically constrained, testable, and resilient to the most predictable reviewer objections.

7.4 Positioning Relative to Existing Theories

CRN is intended to complement, rather than replace, established accounts of decision-making such as attractor networks, drift–diffusion models, and winner-take-all circuits. Those models primarily describe the commitment phase, where a dominant pattern has already begun to emerge and populations actively compete via spiking and

inhibition. CRN targets an earlier bottleneck: pre-selection under communication-dominant energetics, where driving all candidate hypotheses into a high-spiking regime would be metabolically prohibitive.

Relative to classical attractor dynamics, the key architectural claim is that much of hypothesis filtering can occur in a transient subthreshold regime, before irreversible fixation. In CRN, phase-sensitive wave interference performs low-cost suppression of inconsistent candidates, so that only a sparse subset reaches the thresholded readout stage. This framing avoids a straw-man 'full brute-force search': the baseline challenge is not that the brain enumerates every hypothesis serially, but that even energy-efficient attractor implementations can require broad population-level spiking during convergence when the candidate set is large.

Drift–diffusion and related race models inherit this limitation at the level of aggregate dynamics: while they provide accurate fits to psychometric and chronometric data, they typically treat diffusion and threshold parameters phenomenologically and do not explicitly track a separate, low-dissipation pre-selection layer that reduces the number of costly broadcast events. In contrast, CRN elevates this separation (wave pre-selection versus thresholded fixation) to an explicit architectural variable constrained by the energy checkpoint χ.

Relative to wave-based and reservoir computing approaches (including coupled-oscillator analog computing, photonic reservoirs, and coherent oscillator/Ising-inspired optimizers), CRN shares the use of coherent substrate dynamics but adds two ingredients that are central for neurobiological plausibility. First, it treats the communication/computation asymmetry as a first-class constraint and introduces an explicit energy checkpoint (χ) that can, in principle, be falsified by metabolic measurements. Second, it provides operational diagnostics tied to the open-system generator itself: the Liouvillian spectral gap $g(\kappa)$ as a convergence-rate marker, and the robustness width W_κ that quantifies how broadly noise-assisted transport persists without fine tuning. In other words, CRN asks not only whether a given physical substrate can implement a rich transient (as in reservoir computing), but whether that transient can be operated in a reset-limited regime with $\chi \ll 1$ under communication-dominant energetics.

Distinction from communication-through-coherence (CTC) / gamma-synchronization accounts. In CTC-style models, gamma phase alignment primarily serves routing and gain control by increasing effective connectivity between areas. CRN instead assigns phase relations a pre-selection role: interference-like cancellation suppresses inconsistent candidates during Stage I, before the irreversible fixation/broadcast. This is compatible with gamma coupling as a candidate substrate; the distinguishing claim is architectural (filtering vs routing), not the carrier itself.

Finally, the GKSL/Lindblad formalism is used here as a modeling tool, not an ontological claim about microscopic quantum degrees of freedom in cortex. In our interpretation, the state variable ρ is an effective descriptor of wave-like population dynamics on a graph (diagonal terms as activation weights; off-diagonals as phase-coherence proxies) whose interaction with noise and readout is conveniently captured by a trace-preserving open-system equation. Accordingly, CRN is compatible with purely classical wave substrates; what matters for the hypothesis is the existence of a transient, low-dissipation wave layer coupled to a thresholded fixation/broadcast mechanism under reset-limited constraints.

7.5 Limitations and Open Questions

We acknowledge several limitations that define the scope of future work:

Classical mimicry: intermediate-noise optima can, in principle, arise in purely classical analog-wave or threshold-noise systems. Accordingly, we frame inference at the architecture level and emphasize dissociation controls, matched transport baselines (Supplementary Note S6), and the energy checkpoint χ (Sections 6.3 and 7.3), rather than microscopic ontology.

Parameter identifiability: many combinations of effective parameters (γ, κ, η) and topology can yield similar behavioral curves. Without combined measurements (energetics + dynamics, and ideally spectral proxies), the model may be only weakly identifiable from behavior alone, which limits parameter-level inference even if qualitative signatures are present.

Scaling Heuristics: Our energy advantage argument relies on the assumption that the wave dynamics scale favorably with N under small-world-like connectivity. While our N = 1000 stress tests provide evidence of robustness across two orders of magnitude in N_active, analytical control of Liouvillian mode structure and energy scaling on realistic whole-brain connectomes remains an open mathematical problem.

Fine-structure is a strong (non-mandatory) prediction. The localized resonance-window pattern in Figure 8 is presented as a conceptual, high-resolution signature: if observed reproducibly, it would provide unusually diagnostic support for a resonant wave-layer contribution. However, its absence - especially under coarse temperature steps, limited statistical power, or biological heterogeneity - should not be treated as falsification of the CRN architecture. In this work, minimal falsification rests on the broader ENAQT-like / noise-assisted transport (NAT) markers (P1-P2) and the reset/noise dissociation logic (P3) rather than on the fine structure itself.

7.6 Conclusion

The brain faces a stark engineering reality: communication is orders of magnitude more expensive than computation. The Coherent Resonant Netting (CRN) hypothesis proposes that evolution has navigated this bottleneck by adopting a two-stage architecture: a low-cost, transient wave-dynamical layer for pre-selection, coupled to a high-cost, thresholded readout. By exploiting noise as a resource via an ENAQT-like / noise-assisted transport (NAT) mechanism, this architecture can reduce the overall metabolic cost per selection act (quantified here via E_{tax}; Section 6.3). We have formalized this model using open-system (GKSL/Lindblad) dynamics, demonstrated its robustness in silico, and derived strict falsifiability criteria. CRN thus offers a physically grounded, experimentally testable framework that bridges the gap between the abstract normative goals of active inference and the thermodynamic constraints of biological hardware. The primary empirical target of this framework is the architectural hypothesis H_wave—a transient, wave-mediated pre-selection layer under communication-dominant energetics—rather than any specific microscopic quantum ontology.

Data Availability Statement

The full simulation code, figure-generation scripts, and numerical artifacts supporting the computational results are provided as a self-contained Supplementary Simulation Suite (R12-CROWN), archived on Zenodo (concept DOI: 10.5281/zenodo.18338260; version used here: 10.5281/zenodo.18338261).

Funding

No external funding was received for this work.

Conflict of Interest

The author declares no competing interests.

Author Contributions

OD conceived the work, developed the model, performed the simulations, and wrote the manuscript.

Abbreviations

CRN – Coherent Resonant Netting

ENAQT – Environment-Assisted Quantum Transport

NAT – Noise-Assisted Transport (ENAQT-like / noise-assisted transport (NAT) regime)

GKSL – Gorini–Kossakowski–Sudarshan–Lindblad

BAC – Backpropagation-Activated Ca2+ (burst initiation mechanism)

FEP – Free Energy Principle

GNW – Global Neuronal Workspace

GWT – Global Workspace Theory

IIT – Integrated Information Theory

FWHM – Full Width at Half Maximum

WTA – Winner-Take-All

DDM – Drift-Diffusion Model

Q10 – Temperature coefficient for rate scaling

ATP – Adenosine triphosphate

Acknowledgments

The author thanks colleagues and reviewers who provided critical feedback on early versions of the manuscript; any remaining errors are the author's responsibility.

References

Anastassiou, C. A., Perin, R., Markram, H., and Koch, C. (2011). Ephaptic coupling of cortical neurons. Nature Neuroscience 14, 217-223. doi: 10.1038/nn.2727.

Anokhin, K. V. (2021). The cognitome: seeking the fundamental neuroscience of a theory of consciousness. Neuroscience and Behavioral Physiology 51, 915-937. doi: 10.1007/s11055-021-01149-4.

Attwell, D., and Laughlin, S. B. (2001). An energy budget for signaling in the grey matter of the brain. Journal of Cerebral Blood Flow and Metabolism 21, 1133-1145. doi: 10.1097/00004647-200110000-00001.

Bennett, C. H. (1973). Logical reversibility of computation. IBM Journal of Research and Development 17, 525-532. doi: 10.1147/rd.176.0525.

Breuer, H.-P., and Petruccione, F. (2002). The Theory of Open Quantum Systems. Oxford: Oxford University Press.

Caruso, F., Chin, A. W., Datta, A., Huelga, S. F., and Plenio, M. B. (2009). Highly efficient energy excitation transfer in light-harvesting complexes: the fundamental role of noise-assisted transport. The Journal of Chemical Physics 131, 105106. doi: 10.1063/1.3223548.

Engel, G. S., Calhoun, T. R., Read, E. L., Ahn, T.-K., Mančal, T., Cheng, Y.-C., and Fleming, G. R. (2007). Evidence for wavelike energy transfer through quantum coherence in photosynthetic systems. Nature 446, 782-786. doi: 10.1038/nature05678.

Friston, K. (2010). The free-energy principle: a unified brain theory? Nature Reviews Neuroscience 11, 127-138. doi: 10.1038/nrn2787.

Gorini, V., Kossakowski, A., and Sudarshan, E. C. G. (1976). Completely positive dynamical semigroups of N-level systems. Journal of Mathematical Physics 17, 821-825. doi: 10.1063/1.522979.

Inagaki, T., Inaba, K., Hamerly, R., Inoue, K., Yamamoto, T., Takesue, H., et al. (2016). A coherent Ising machine for 2000-node optimization problems. Science 354, 603-606. doi: 10.1126/science.aah4243.

Jefferys, J. G. R. (1995). Nonsynaptic modulation of neuronal activity in the brain: electric currents and extracellular ions. Physiological Reviews 75, 689-723. doi: 10.1152/physrev.1995.75.4.689.

Kitamoto, T. (2001). Conditional modification of behavior in Drosophila by targeted expression of a temperature-sensitive shibire allele in defined neurons. Journal of Neurobiology 47, 81-92. doi: 10.1002/neu.1018.

Landauer, R. (1961). Irreversibility and heat generation in the computing process. IBM Journal of Research and Development 5, 183-191. doi: 10.1147/rd.53.0183.

Larkum, M. E. (2013). A cellular mechanism for cortical associations: an organizing principle for the cerebral cortex. Trends in Neurosciences 36, 141-151. doi: 10.1016/j.tins.2012.11.006.

Lennie, P. (2003). The cost of cortical computation. Current Biology 13, 493-497. doi: 10.1016/S0960-9822(03)00135-0.

Lin, X., Rivenson, Y., Yardimci, N. T., Veli, M., Luo, Y., Javed, A., et al. (2018). All-optical machine learning using diffractive deep neural networks. Science 361, 1004-1008. doi: 10.1126/science.aat8084.

Lindblad, G. (1976). On the generators of quantum dynamical semigroups. Communications in Mathematical Physics 48, 119-130. doi: 10.1007/BF01608499.

Marandi, A., Wang, Z., Takata, K., Byer, R. L., and Yamamoto, Y. (2014). Network of time-multiplexed optical parametric oscillators as a coherent Ising machine. Nature Photonics 8, 937-942. doi: 10.1038/nphoton.2014.249.

Plenio, M. B., and Huelga, S. F. (2008). Dephasing-assisted transport: quantum networks and biomolecules. New Journal of Physics 10, 113019. doi: 10.1088/1367-2630/10/11/113019.

Rebentrost, P., Mohseni, M., and Aspuru-Guzik, A. (2009). Role of quantum coherence and environmental fluctuations in chromophoric energy transport. Journal of Physical Chemistry B 113, 9942-9947. doi: 10.1021/jp901724d.

Takahashi, N., Oertner, T. G., Hegemann, P., and Larkum, M. E. (2016). Active cortical dendrites modulate perception. Science 354, 1587-1590. doi: 10.1126/science.aah6066.

Tononi, G. (2008). Consciousness as integrated information: a provisional manifesto. The Biological Bulletin 215, 216-242. doi: 10.2307/25470707.

Van der Sande, G., Brunner, D., and Soriano, M. C. (2017). Advances in photonic reservoir computing. Nanophotonics 6, 561-576. doi: 10.1515/nanoph-2016-0132.

Vandoorne, K., Mechet, P., Van Vaerenbergh, T., Fiers, M., Morthier, G., Verstraeten, D., et al. (2014). Experimental reservoir computing in photonics. Nature Communications 5, 3541. doi: 10.1038/ncomms4541.

Watts, D. J., and Strogatz, S. H. (1998). Collective dynamics of 'small-world' networks. Nature 393, 440-442. doi: 10.1038/30918.

Yamamoto, Y., Leleu, T., Rahman, A., Aihara, K., Kawarabayashi, K., Kako, S., et al. (2017). Coherent Ising machines: optical neural networks operating at the quantum limit. npj Quantum Information 3, 49. doi: 10.1038/s41534-017-0048-9.

Figure Captions

Figure 1 | CRN architecture and temporal/energetic hierarchy. (A) A cognitome graph G = (V, E) encodes the structured hypothesis space. At any decision act, only a sparse active subgraph is recruited ($N_{active} \ll N_{total}$) and biased by a diagonal potential V (free-energy / prediction-error proxy). (B) Two-stage decision cycle. Stage I performs wave-mediated pre-selection on the active subgraph via GKSL dynamics (under dephasing κ and a sink/readout channel), suppressing inconsistent hypotheses via interference. Once a candidate crosses threshold, Stage II implements irreversible fixation (sink capture) that gates spike-based long-range broadcast (communication-dominant cost E_{comm}) and updates priors V for the next episode. (C) Schematic hierarchy: transport is fast (τ_{trans}), while throughput is reset-limited ($\tau_{reset} \gg \tau_{trans}$). Per-act energy decomposes as $E_{CRN} = E_{pre} + E_{readout} + E_{comm}$, with $E_{pre} \ll N_{active} \cdot E_{comm}$. Numeric values shown in Panel C are illustrative and not to scale.

Figure 2 | Noise-assisted transport on a minimal graph (N=10 chain). The Liouvillian spectral gap $g(\kappa)$ versus dephasing rate κ (γ=4.0, η=0.8) exhibits three regimes: low-κ interference trapping (small gap), an intermediate-noise ENAQT-like / noise-assisted transport (NAT) window with a maximum at $\kappa=\kappa^*$, and a high-κ overdamped (Zeno/diffusive) regime where the gap decreases. The functional window width is $W_\kappa = \log10(\kappa_{hi}/\kappa_{lo})$ at half maximum (FWHM on a log10 κ axis).

Figure 3 | Large-scale robustness on a Watts–Strogatz small-world network (N=1000). The finite-horizon success probability $P_{success}(T)$ is non-monotonic in κ, showing an intermediate-noise ENAQT-like / noise-assisted transport (NAT) window. Shaded band: ±1 SD over graph realizations. The functional width is reported as the FWHM on a log10 κ axis.

Figure 4 | Topology robustness of the ENAQT-like / noise-assisted transport (NAT) spectral marker (N=10). Normalized Liouvillian gap curves $g(\kappa)/g(\kappa^*)$ versus κ/κ^* for chain, Watts–Strogatz, and modular graphs (γ=4.0, η=0.8) show substantial collapse, suggesting that the intermediate-noise optimum is compatible with multiple coarse circuit/connectome motifs.

Figure 5 | Robustness to thresholded readout in the large-N proxy (N=1000). Success traces $P_{success}(t)=1-||\psi(t)||$ ^2 for linear and thresholded sinks at an intermediate-noise setting (κ=1.0). The thresholded readout activates after the target intensity crosses a threshold (vertical marker), delaying but not eliminating the monotonic rise in success.

Figure 6 | Reset bottleneck and energy checkpoint. As τ_{reset} increases (reset-limited regime), the act rate $f_{fix} \approx 1/\tau_{reset}$ decreases, raising the per-act wave-layer tax $E_{tax}=P_{tax}/f_{fix}$. The dimensionless checkpoint $\chi=E_{tax}/E_{comm}$ is

shown with illustrative safe and red-line bands; CRN's energetic advantage requires $\chi \ll 1$ and is treated as practically absent for $\chi \gtrsim 0.1$.

Figure 7 | Drosophila dissociation protocol and falsification logic. A behavioral anesthesia-recovery assay provides a tractable readout (latency distribution $P_{rec}(t)$ and tail quantiles). Noise-proxy manipulations (κ, e.g., temperature scans or pharmacological noise modulators) are predicted to yield a non-monotonic ENAQT-like / noise-assisted transport (NAT) profile with an intermediate-noise optimum; the functional window width W_{κ} can be estimated from the κ-latency curve. Reset-proxy manipulations (τ_{reset}, e.g., shi^{ts1}/para mutants or dose-dependent recovery kinetics) should primarily shift throughput/latency via $f_{fix} \approx 1/\tau_{reset}$, with minimal change in the κ-optimum/curve shape. Falsification corresponds to monotonic improvement as noise is reduced, or indistinguishable effects of "noise" and "reset" manipulations.

Figure 8 | Optional fine-structure prediction (conceptual sketch). A purely biochemical recovery model predicts a smooth Arrhenius/Q10-like dependence of recovery speed on temperature (dashed curve). CRN allows, as a strong but non-mandatory signature, localized resonance windows: narrow temperature bands where recovery speed (e.g., 1/τ_reset) deviates sharply from the smooth baseline (solid curve). This fine structure is intended as a high-resolution follow-up marker: its presence would be highly informative, whereas its absence in coarse initial experiments does not falsify the minimal CRN predictions.